Clinical and Translational Radiation Oncology 17 (2019) 32–39

Contents lists available at ScienceDirect

Clinical and Translational Radiation Oncology

journal homepage: www.elsevier.com/locate/ctro

Original Research Article

Computer-assisted image analysis of the tumor microenvironment on an oral tongue squamous cell carcinoma tissue microarray

Sangjune Laurence Lee [a], Michael Cabanero [b,c], Martin Hyrcza [b,c], Marcus Butler [c,d], Fei-Fei Liu [a,c], Aaron Hansen [c,d], Shao Hui Huang [a,c], Ming-Sound Tsao [b,c], Yuyao Song [c,e], Lin Lu [c,e], Wei Xu [c,e], Douglas B. Chepeha [c,f], David P. Goldstein [c,f], Ilan Weinreb [b,c], Scott V. Bratman [a,c,g,*]

[a] Department of Radiation Oncology, University of Toronto, Canada
[b] Department of Laboratory Medicine and Pathobiology, University of Toronto, Canada
[c] Princess Margaret Cancer Centre, University Health Network, Canada
[d] Department of Medical Oncology, University of Toronto, Canada
[e] Department of Biostatistics, University of Toronto, Canada
[f] Department of Otolaryngology, University of Toronto, Canada
[g] Department of Medical Biophysics, University of Toronto, Canada

ARTICLE INFO

Article history:
Received 15 February 2019
Revised 9 May 2019
Accepted 12 May 2019
Available online 18 May 2019

ABSTRACT

Oral tongue squamous cell carcinoma (OTSCC) displays variable levels of immune cells within the tumor microenvironment. The quantity and localization of tumor infiltrating lymphocytes (TILs), specific functional TIL subsets (e.g., CD8+), and biomarker-expressing cells (e.g., PD-L1+) may have prognostic and predictive value. The purpose of this study was to evaluate the robustness and utility of computer-assisted image analysis tools to quantify and localize immunohistochemistry-based biomarkers within the tumor microenvironment on a tissue microarray (TMA). We stained a 91-patient OTSCC TMA with antibodies targeting CD3, CD4, CD8, FOXP3, IDO, and PD-L1. Cell populations were segmented into epithelial (tumor) or stromal compartments according to a mask derived from a pan-cytokeratin stain. Definiens Tissue Studio was used to enumerate marker-positive cells or to quantify the staining intensity. Automated methods were validated against manual tissue segmentation, cell count, and stain intensity quantification. Univariate associations of cell count and stain intensity with smoking status, stage, overall survival (OS), and disease-free survival (DFS) were determined. Our results revealed that the accuracy of automated tissue segmentation was dependent on the distance of the tissue section from the cytokeratin mask and the proportion of the tissue containing tumor vs. stroma. Automated and manual cell counts and stain intensities were highly correlated (Pearson coefficient range: 0.46–0.90; $p < 0.001$). Within this OTSCC cohort, smokers had significantly stronger PD-L1 stain intensity and higher numbers of CD3+, CD4+ and FOXP3+ TILs. In the subset of patients who had received adjuvant radiotherapy, a higher number of CD8+ TILs was associated with inferior OS and DFS. Taken together, this proof-of-principle study demonstrates the robustness and utility of computer-assisted image analysis for high-throughput assessment of multiple IHC markers on TMAs, with potential implications for studies on prognostic and predictive biomarkers.

1. Introduction

Oral cavity cancer is estimated to cause 128,000 deaths annually worldwide. Despite advances in diagnostic and therapeutic approaches, mortality rates of oral cavity squamous cell carcinoma (OTSCC), which make up 90% of all oral neoplasms, have not improved significantly during the last 30 years with a 5-year survival of 40–50% [1–3]. The effect of treatment regimen or other prognosis-related factors is often uncertain and controversial in this disease [4].

Prognostic and predictive biomarkers hold the promise to enable more personalized treatment of OTSCC in order to improve cure rates and minimize side effects. In addition to the tumor, node, and metastases (TNM) staging system, recent studies suggest that the tumor immune microenvironment may provide independent prognostic information [5]. OTSCC is among the most highly immune-infiltrated cancer types [6]. The density of tumor infiltrat-

* Corresponding author at: 610 University Ave, Toronto, ON M5G 2M9, Canada.
E-mail address: Scott.Bratman@rmp.uhn.ca (S.V. Bratman).

https://doi.org/10.1016/j.ctro.2019.05.001

ing lymphocytes (TILs) and their exact location within the epithelium or stroma within tumors may be prognostic [7]. Moreover, the presence and distribution of TILs and TIL subsets within tumors may be predictive of response to immune checkpoint inhibitors such as antibodies targeting the PD-1/PD-L1 axis [8].

Immunohistochemistry (IHC) is a semiquantitative diagnostic technique that is routinely used in clinical surgical pathology to evaluate various tumor markers including components of the tumor immune microenvironment [9]. Multiple tumor samples may be stained by IHC and evaluated in a consistent manner using tissue microarrays (TMA). Although TMAs can facilitate throughput of tissue staining, manual reading of IHC studies evaluating protein expression on TMAs is labor intensive and prone to bias [10,11]. Biomarker studies on the tumor immune microenvironment have shown conflicting results at times, which could be attributed to the absence of validated and standardized quantification methods [11,12].

The use of computer-assisted image analysis may enable high-throughput quantitative analysis of IHC on TMAs. Studies have demonstrated the use of computer-assisted image analysis in the quantification of cell count [13,14] and automated segmentation of tissue compartments [15]. In order to localize immune cells to tissue compartments, software packages have used digital pattern recognition [16].

We hypothesized that computer-assisted image analysis of IHC can be used for robust quantification and localization of TILs, TIL subsets, and related biomarker-expressing cells within the tumor microenvironment. Our objective was to validate the use of computer image analysis tools using a TMA of OTSCC. The prognostic implications of these immune markers were then explored.

2. Materials and methods

2.1. Study patients

Patients with OTSCC treated at our institution were included in this retrospective cohort study. Each patient had a biopsy sample taken from the primary tumor site in the oral cavity. Patients were treated with definitive surgical resection of primary ± neck dissection. Decision of adjuvant treatment was determined in multidisciplinary setting and adjuvant radiotherapy with or without concurrent cisplatin chemotherapy was typically given for patient with adverse pathologic features, according to NCCN guidelines such as pT3-4, close resection margins less than 5 mm, lymphovascular invasion (LVI), perineural invasion (PNI), multiple positive lymph nodes, pathological extranodal extension and positive resection margins. The latter two were considered high-risk features and merit addition of chemotherapy [17]. An experienced head and neck pathologist (I.W.) reviewed all cases for diagnosis and grade. The WHO 2005 classification was used, which is also consistent with the WHO 2017 classification. Demographic, clinical, and outcome data were prospectively collected at the point-of-care.

2.2. TMA preparation and Immunohistochemistry

A tissue microarray (TMA) was built from 182 samples of OTSCC, 2 samples each from 91 patients managed at a Canadian tertiary academic oncology center who consented to being included in a clinical database of patients with newly diagnosed previously untreated OTSCC and in whom adequate tissue was available. Specimens were retrieved from the institution's biobank repository and, if not available in the biobank, from archived pathology specimens. All tumor specimens were preserved in formalin fixed blocks. For each tumor, two duplicate 0.6 mm cores of tumor were included in the TMA.

The immune markers shown in Table 1 were used to label the TMA on serial 4 μm thick tissue sections with brown chromogen stain and hematoxylin counterstain. IHC was performed at *Princess Margaret Cancer Center Advanced Molecular Profiling Lab (AMPL)* core facility. TMA paraffin sections at 4 μm thickness were dried at 60 °C oven overnight before staining. The IHC was performed according to the manufacture's guidelines using BenchMark XT-an automated slide strainer (Ventana Medical System) with standard antigen retrieval (CC1, Tris/Borate/EDTA pH8.0, #950-124) or with protease1 (760–2018) for 4 min. The origin and dilution of the antibodies used for IHC were as follows: anti-CD3 rabbit monoclonal (Ventana/Roche, 2GV6) for 30 min; anti-CD4 rabbit monoclonal (Ventana/Roche, SP35), anti-CD8 rabbit monoclonal (Ventana/Roche, SP57), anti-FOXP3 mouse monoclonal (Abcam, 236A/E7) at 1:100 dilution, and anti-IDO mouse monoclonal (Millipore, 1F8.2) at 1:300 dilution for 60 min; and anti-PD-L1 rabbit monoclonal (CST, E1L3N) at 1:100 dilution for 90 min. Ventana Ultraview Universal DAB Detection Kit (#760-500) containing a cocktail of labeled secondary antibodies was then utilized. The complex was visualized with hydrogen peroxide substrate and 3,3′-diaminobenzidine tetrahydrochloride (DAB) chromogen. The slides were counterstained with Ventana Hematoxylin II and Bluing reagent, dehydrated in graded alcohol, cleared in xylene and coverslipped in Permount. Downstream analysis was performed on those TMA cores that passed initial quality assessment, including adequate sample area (>75% of that expected for a 0.6 mm diameter core) and lack of sectioning artefacts.

2.3. Computer-assisted image analysis

IHC stained TMA slides were digitized with a magnification of 20× using Aperio Scanscope XT (Leica Biosystems Inc., Buffalo Grove, USA). Tissue Studio (Definiens AG, Munich, Germany) was used to enumerate the number of marker-positive (CD3+, CD4+, CD8+, or FOXP3+) cells and to quantify the staining intensity for IDO or PD-L1. Stromal or epithelial (tumor) compartments of each core was identified using the cytokeratin section as a tissue mask. Cell populations were localized to either stroma or epithelium after rigidly registering each core with the stain of interest to the cytokeratin section through rotations and translations using a custom Matlab script as shown in Fig. 1.

Table 1
Immunohistochemistry stains used in this study.

Marker	Description	Antibody clone name	Supplier	Clone	Dilution
CD3	T-lymphocytes	anti-CD3 rabbit monoclonal	Ventana/Roche	2GV6	
CD4	helper T-cells	anti-CD4 rabbit monoclonal	Ventana/Roche	SP35	
CD8	cytotoxic T-cells	anti-CD8 rabbit monoclonal	Ventana/Roche	SP57	
FOXP3	regulatory T-cells	anti-FOXP3 mouse monoclonal	Abcam	236A/E7	1:100
IDO	Immune suppressive molecule present on dendritic cells, monocytes and macrophages	anti-IDO mouse monoclonal	Millipore	1F8.2	1:300 dilution for 60 min
PD-L1	Ligand for PD-1, immune suppressive molecule	anti-PD-L1 rabbit monoclonal	CST	E1L3N	1:100 dilution for 90 min
AE1/AE3	Cytokeratin in epithelial tissue				

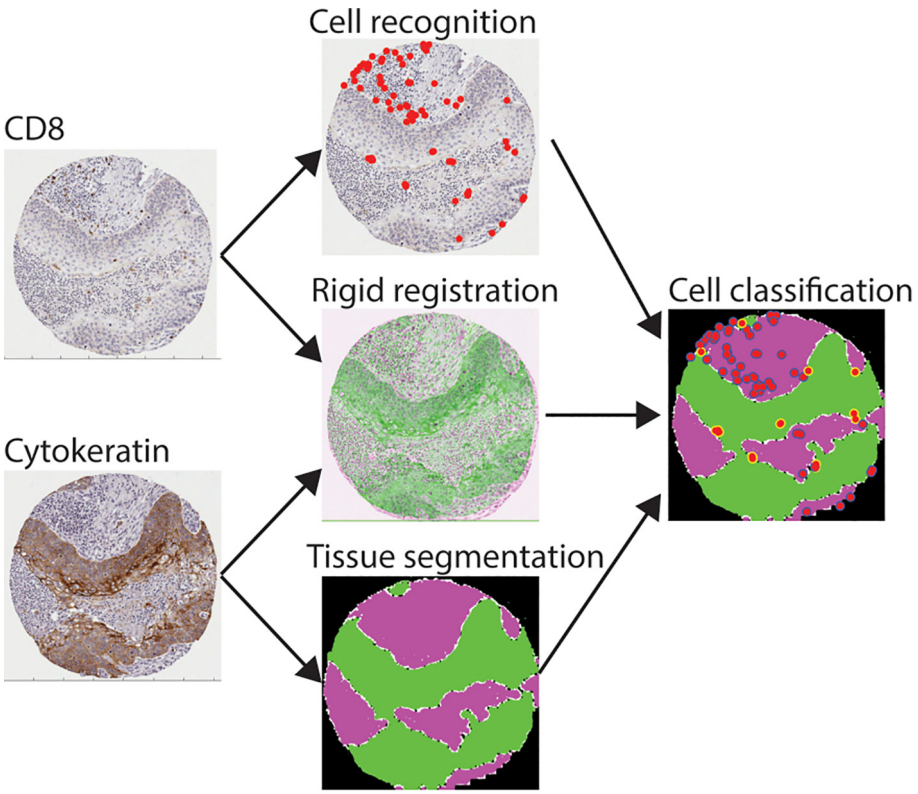

Fig. 1. Image analysis work flow. IHC stain of interest, in this illustration CD8, undergoes either cell recognition or H-scoring. The TMA core section with the stain of interest is registered through rotational and translational movements to the section with the cytokeratin stain. The cytokeratin stain is used to segment the core into either stroma or epithelium. Recognized cells are then placed on the segmentation map to determine localization to either the stroma or epithelium.

2.4. Manual segmentation and IHC scoring

Manual counts of stained cells were performed by a board-certified pathologist (M.C.). The total numbers of CD3+, CD4+, CD8+, and FOXP3+ cells in the epithelial (tumor) and stromal compartments of each TMA core were enumerated. For PD-L1, the intensity and percent of membranous staining of PD-L1+ tumor cells and membranous and/or cytoplasmic staining of immune cells in both epithelial and stromal compartments were used to calculate an H-score for each TMA core. The H-score is calculated as the sum of percent of cells stained at low intensity times 1, percent of cells stained at intermediate intensity times 2, and percent of cells stained at high intensity times 3, with a range of score from 0 to 300 [18]. Clinical PD-L1 scoring methods such as tumour percentage score (TPS), combined positive score (CPS), or immune cell (IC) score were not used as the H-score provided a wider range of scores to accurately describe different staining intensities [19,20]. Nine representative samples (10% of the population), varying in degree of complexity in differentiating epithelium from stroma, were manually segmented to evaluate the robustness of biomarker quantification and localization. Automatic and manual segmentation of the epithelial (tumor) and stroma compartments was performed on each IHC stained section (Fig. 2).

2.5. Statistical analysis

Descriptive statistics are provided with median and range for continuous variables and frequencies and percentages for categorical variables. Demographics and clinical characteristics are compared by Wilcoxon rank sum test for continuous variables and Fisher exact tests for categorical variables. Tissue segmentations were compared between manual and automatic methods using a Dice coefficient measure. The manual FOXP3+ cell counts and PD-L1 H-scores were compared to the automated cell count and H-score using the Pearson correlation coefficient.

Univariate and multivariable Cox proportional hazards models were used to estimate impact of immune markers on OS and DFS. OS and DFS between cohorts were compared by log-rank test. All tests were two-sided. Results were considered significant if the p-value was $\leq$0.05. All statistical analyses are performed using SAS 9.4 and R (R Foundation, Vienna, Austria).

3. Results

3.1. Patient cohort for TMA image analysis

91 patients with OTSCC underwent treatment from 2005 to 2008 consisting of surgery only (n = 59) or followed by adjuvant radiotherapy or cisplatin-based chemoradiotherapy (n = 32) (Table 2). 37 patients were never smokers. A TMA containing 2 cores per tumor was stained with 7 different antibodies by IHC for image analysis (total of 1274 tumor images). 241 (18.9%) of the images were excluded due to inadequate sample area, and 7 (0.5%) samples were excluded due to sectioning artifacts. The remaining 1026 (80.5%) images were used for downstream analysis.

3.2. Segmentation of epithelial and stromal compartments

Segmentation of TMA images into epithelial (tumor) and stromal components is needed for detailed characterization of the tumor microenvironment. We compared our automated computer-assisted tissue segmentation procedure that relied on a separately stained cytokeratin mask to manual analysis performed

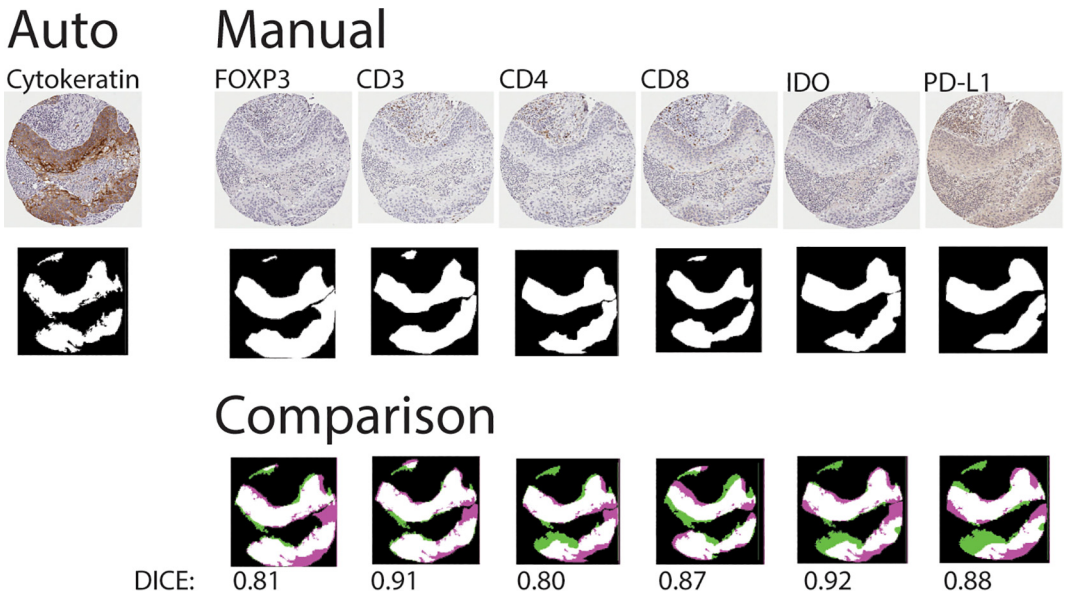

Fig. 2. TMA core segmentation validation. The Dice coefficient was calculated between the automatically segmented epithelium from the cytokeratin section versus the manually segmented epithelium from sections containing the immune stain of interest for nine cores (N = 9), an example of which is shown here. Differences in segmentation are due to changing epithelium distributions with increased distances from the cytokeratin section and challenges in manual contouring. Violet and green represents stroma from the automatic and manual segmentation, respectively. (For interpretation of the references to colour in this figure legend, the reader is referred to the web version of this article.)

Table 2
Demographics of oral squamous cell carcinoma patients. Abbreviations: SD = standard deviation, RT = radiation therapy, CRT = chemoradiation therapy.

Variables	n = 91 (100%)
Age	
Mean (SD)	59.6 (14.8)
Median (Min,Max)	60.4 (20.7,87.3)
Gender	
Female	43 (47)
Male	48 (53)
Smoking History	
Current	35 (40)
Never	37 (41)
Non/Ex-Smoker	53 (60)
Missing	3
Stage	
I	25 (27)
II	25 (27)
III	12 (13)
IVA	28 (31)
IVC	1 (1)
Treatment	
Surgery Only	59 (65)
Adj. RT	20 (22)
Adj. CRT	12 (13)
Follow Up Alive	
Mean (SD)	6.1 (2.7)
Median (Min,Max)	6.2 (0.3,10.9)
Missing	35
Recurrences	41 (45)
Deaths	35 (38)

on each TMA section (Fig. 2). Agreement between automated and manual tissue segmentation results were variable (Dice coefficient range 0.45–0.95; mean ± standard deviation 0.70 ± 0.15).

We next explored factors that influenced the accuracy of segmentation. Automated segmentation of the epithelial compartment declined in accuracy with increasing distance from the cytokeratin section and with decreasing epithelial tissue area (Figs. 3 and 4). Agreement between automated and manual segmentation was higher when both were performed on the same cytokeratin section than when the automated segmentation was performed on the cytokeratin section and the manual segmentation was performed on a different section taken from the same core (Dice coefficient mean ± standard deviation 0.85 ± 0.06 vs. 0.70 ± 0.15, p = 0.002).

3.3. Comparison of automated versus manual IHC stain scoring on the TMA

We conducted a comparative analysis of automated versus manual biomarker quantification within the tumor microenvironment. For this, we used FOXP3 and PD-L1 to represent cell count and continual staining intensity (H-score), respectively. FOXP3+ cell count and PD-L1 H-score were determined using automated and manual methods for 149 (81.9%) and 143 (78.6%) of the samples with adequate cores (sufficient area and no sectioning artifacts), respectively. As shown in Fig. 5, automated and manual FOXP3+ cell counts had a correlation of R = 0.56 ($p = 2.5 \times 10^{-12}$) in the epithelium and R = 0.90 ($p = 5.8 \times 10^{-54}$) in the stroma. Automated and manual PD-L1 H-score had a correlation of R = 0.46 ($p = 5.0 \times 10^{-8}$) in the epithelium and R = 0.51 ($p = 3.0 \times 10^{-10}$) in the stroma. These results suggest that automated computer-assisted image analysis of this OTSCC TMA produces cell counts and H-score results that correlate with manual quantification.

3.4. Automated computer-assisted image analysis of OTSCC tumor microenvironment

Next, we used the automated computer-assisted image analysis of the OTSCC TMA to evaluate putative biomarkers within the tumor microenvironment. Specifically, we assessed the correlation of the infiltrating immune cell counts and staining intensities within the segmented epithelial and stromal compartments (Fig. 6). In the stromal compartment, CD3+, CD4+, CD8+ and FOXP3+ cell counts were strongly correlated with one another (Pearson R = 0.6–0.95; $p < 1.0 \times 10^{-15}$ for all), and PD-L1 H-score and CD8+ cell counts were moderately correlated with one another

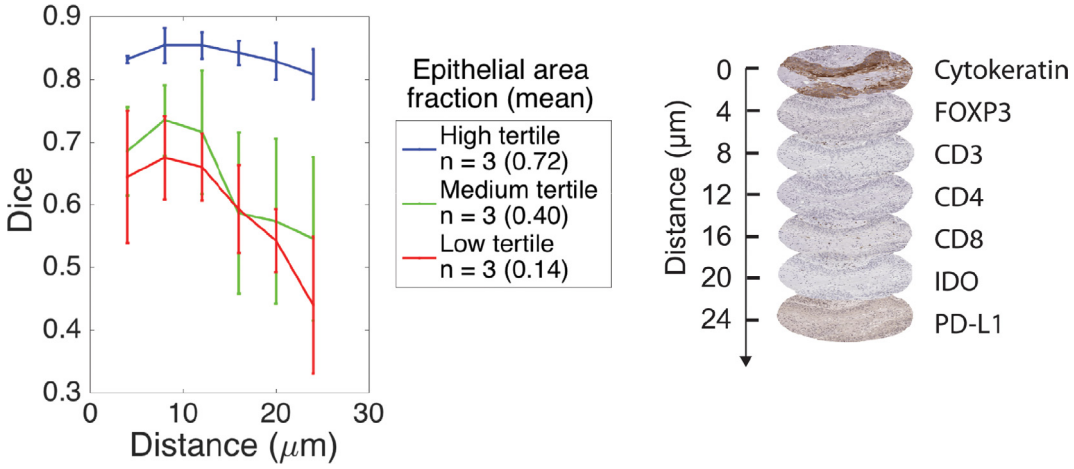

Fig. 3. Epithelial tissue segmentation accuracy depends on distance from cytokeratin section and relative epithelial area. For each of the nine representative segmented samples, the epithelial component of each section of interest was compared to the automatically segmented epithelial component of the respective cytokeratin section. Mean Dice coefficient decreases as the distance from the cytokeratin section increases. Accuracy also falls as the epithelial proportion of the total core area decreases. Error bars indicate ± one standard deviation.

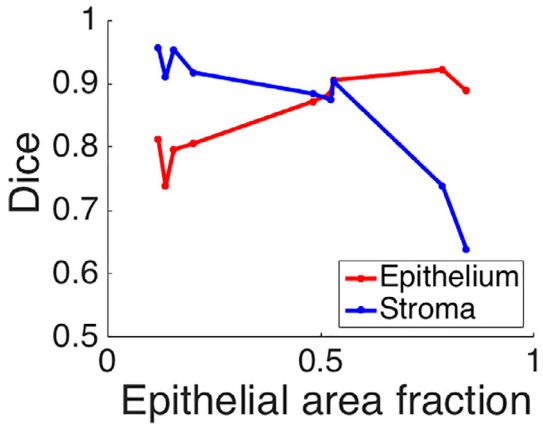

Fig. 4. Segmentation accuracy versus relative tissue area. 9 representative samples were selected and the cytokeratin section was both automatically and manually segmented. The Dice coefficients comparing the two were calculated. As the epithelial proportion of the total core area increases, accuracy of epithelial tissue segmentation increases. Conversely, as the epithelial proportion of the total core area increases (i.e. stromal proportion of the total core area decreases) and accuracy of stromal tissue segmentation decreases.

($R > 0.6$; $p < 1.0 \times 10^{-9}$). In contrast, in the epithelial compartment, CD3+, CD4+, CD8+ and FOXP3+ cell counts had weak correlations in the epithelium ($R < 0.3$; p ranging between 1.0×10^{-3} to 0.9).

Compared to never-smokers, current and ex-smokers had a significantly increased number of CD3+, CD4+, and FOXP3+ cells in the epithelial compartment (OR = 1.003, 1.004, 1.023 p = 0.036, 0.017, 0.022 respectively), and had a trend towards stronger PD-L1 stain intensity in both epithelial and stromal compartments (OR = 1.025, 1.019; p = 0.079, 0.053 respectively); these results were confirmed by manual scores (Supplementary Tables S1–S2). No significant correlations were found between the immune markers of interest and overall stage, N stage, and T stage.

3.5. Prognostic significance of TILs in OTSCC

We next performed an exploratory analysis to identify prognostic biomarkers in this OTSCC cohort. Few statistically significant correlations were observed (Tables S3–S4). Among patients treated with adjuvant radiotherapy (n = 27), high levels of infiltrating (i.e., in the epithelial compartment) CD8+ cells was associated with inferior OS (HR = 1.003, 95% CI: 1.000–1.005, p = 0.03) and DFS (HR = 1.002, 95% CI: 1.000–1.005, p = 0.04) (Fig. 7 and Supplementary Figs. S1–S2). There was a statistically significant interaction effect between epithelial CD8+ cell count and treatment with adjuvant radiotherapy (p = 0.016 for OS, p = 0.0025 for DFS) (Table S5).

4. Discussion

Understanding the distribution and location of immune cells and immune system signaling cell markers within the microenvironment of head and neck cancers may help identify prognostic and predictive biomarkers. Manual scoring of IHC results is labor intensive and susceptible to interobserver and intraobserver variability. Standardization of IHC immune marker scoring through automation for high-throughput analysis of TMAs may facilitate the discovery of these biomarkers. In this work, we demonstrate the use of computer-assisted image analysis on a 91-patient OTSCC TMA to automatically segment epithelial and stromal tissue compartments and determine immune cell count and cell staining intensity. From our exploratory analysis, we show that infiltrating immune cell density and PD-L1 staining intensity is higher in smokers compared to non-smokers. Furthermore, we show that among patients treated with adjuvant radiotherapy, high levels of infiltrating CD8+ cells were associated with a detriment in OS and DFS.

Various studies have demonstrated the use of computer-assisted image analysis to quantify tissue segmentation [16], marker staining intensity [15,21,22] and cell count [13,14,23,24]. Smaller studies have shown image analysis algorithms are more accurate than manual IHC scoring [25]. Despite the abundance of these studies as well as open source and commercially available software, including some FDA approved software packages, the College of American Pathologists and American Society of Clinical Oncology has stated that there is no universally acceptable procedure for validating digital imaging methods [26].

We used Definiens image analysis software as it has been reported to accurately segment tissue compartments and has been used in colorectal cancer "Immunoscore" analysis [25,27,28]. However, in our experience, Definiens digital pattern recognition was unable to consistently identify epithelial and stromal compartments of OTSCC from IHC slides. To improve performance, in this study we utilized a mask from a separate tissue section stained

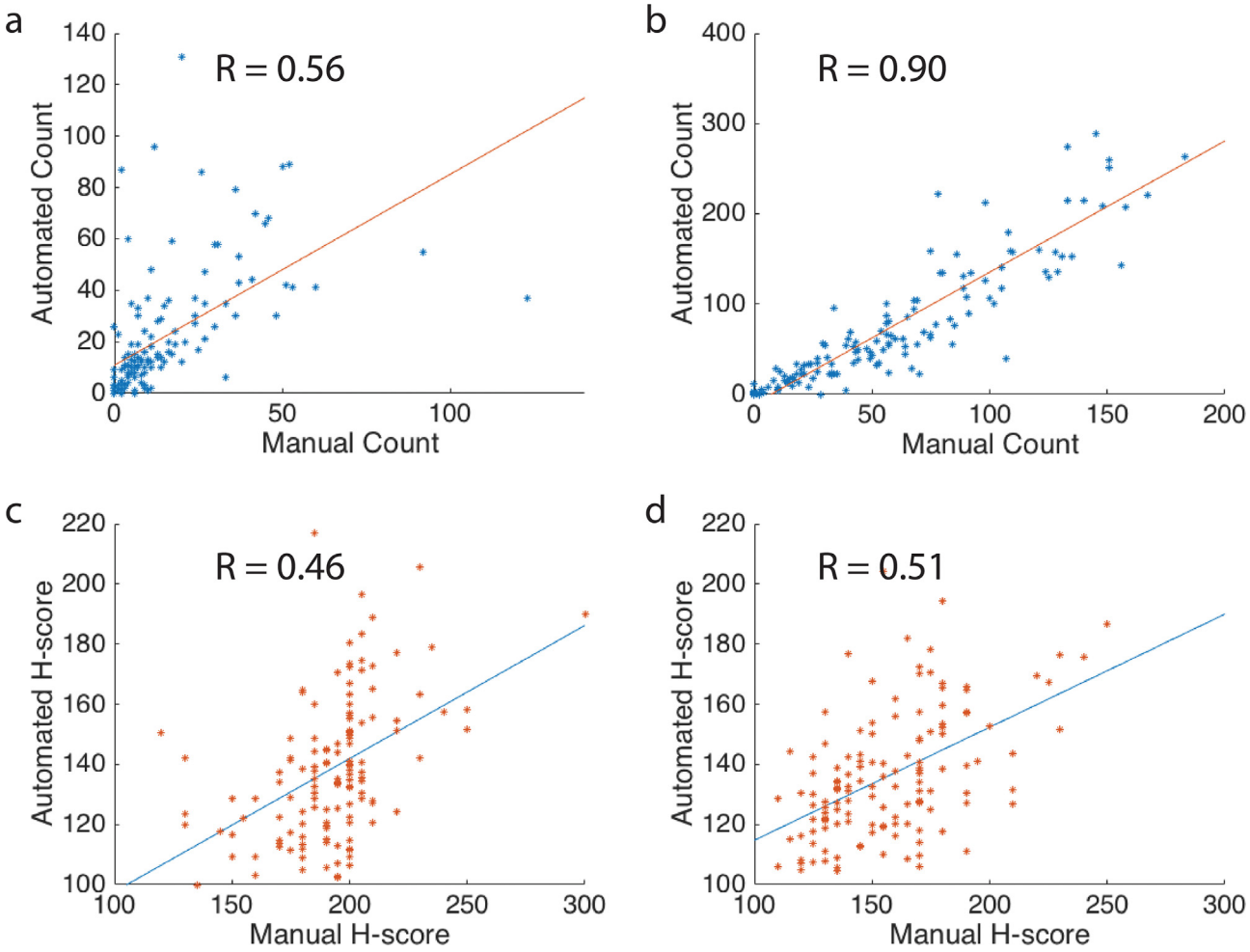

Fig. 5. Automated scoring versus manual scoring of cell counts and staining intensities. (a) FOXP3+ cell count in the epithelial, (b) FOXP3+ cell count in the stromal compartment, (c) PD-L1 H-score in the epithelial compartment, and (d) PD-L1 H-score in the stromal compartment.

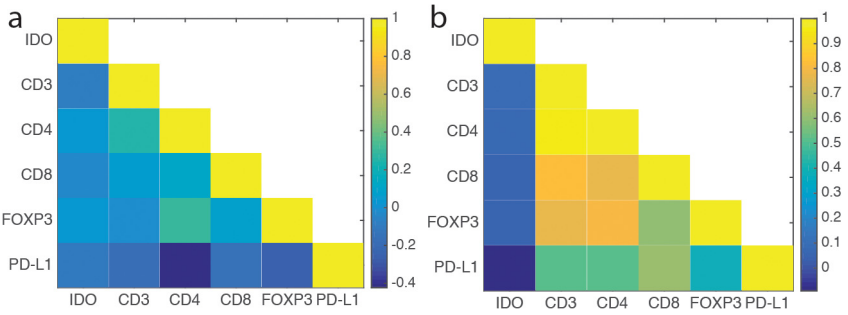

Fig. 6. Relationships between TIL subsets and biomarker expression. Pearson correlation coefficient comparing cell counts for IDO+, CD3+, CD8+, FOXP3+ cells and H-Score for PD-L1 in (a) the epithelial compartment and (b) the stromal compartment.

with pan-cytokeratin antibodies in order to distinguish the epithelial tumor compartment from the surrounding stroma. We found that segmentation accuracy was generally good using this approach, but accuracy declined for sections that were serially further from the cytokeratin-stained section or that consisted of a low proportion of the tissue compartment of interest. In future studies, cytokeratin stained sections taken at regular intervals along the length of the core sample could compensate for the expected tissue changes and improve the cytokeratin mask.

Having validated the automated computer-assisted method for tissue compartment segmentation, we evaluated the method for quantification of immune cell counts and biomarker staining intensities within the OTSCC tumor microenvironment. We found that the automated method produced cell counts that were more highly correlated with manual cell counts in the stromal compartment than the epithelial compartment. This may be due to more accurate manual cell counts in the stroma of oral cavity squamous cell carcinomas, where greater numbers of lymphocytes are present as compared with the epithelial compartment [29].

While our methods have yet to be validated with other OTSCC cohorts, our exploratory analysis of the immune IHC scores with clinical factors and outcomes produced interesting findings. There were strong correlations between the stromal populations of CD3+, CD4+, CD8+ and FOXP3+ lymphocytes. In smokers, there were

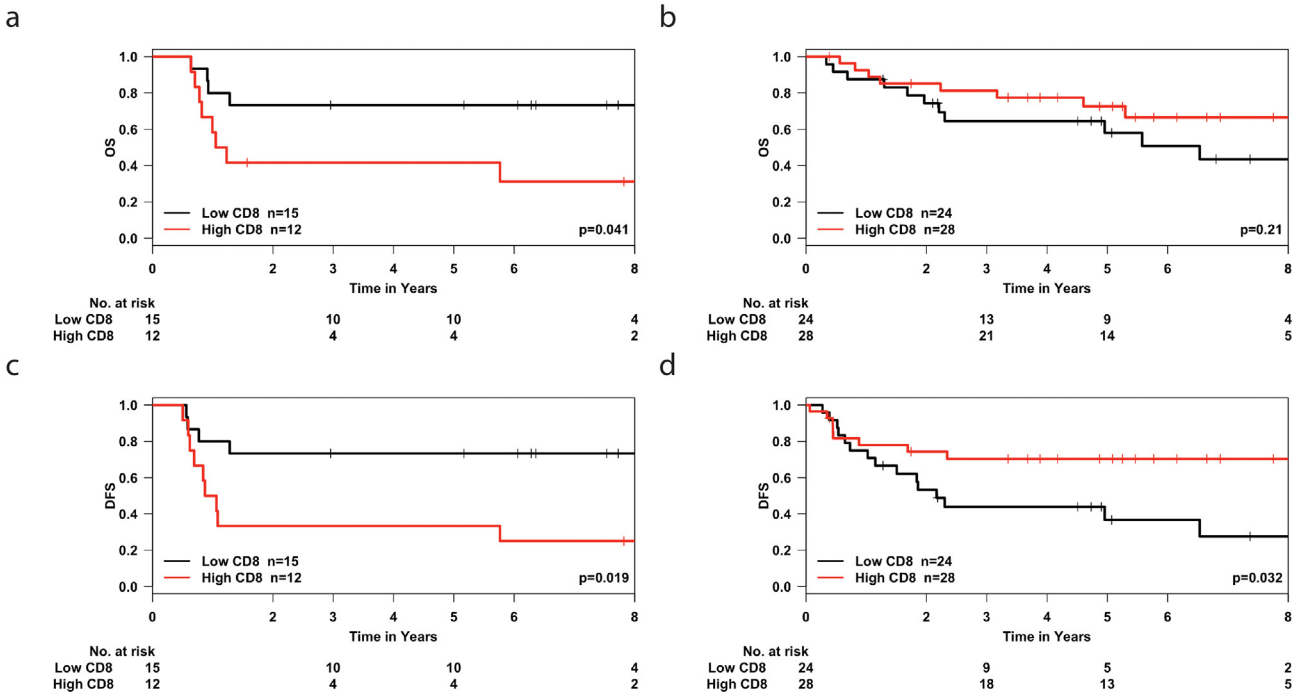

Fig. 7. Prognostic association of putative biomarkers. Epithelial CD8+ count versus OS and DFS with patients dichotomized based on median CD8+ cell count. (a) OS for patients who received radiation, (b) OS for patients who did not receive radiation, (c) DFS for patients who received radiation, and (d) DFS for patients who did not receive radiation. Patients who received radiation therapy with a higher CD8+ count in the epithelium have a lower OS and DFS while patients who did not receive radiation therapy with a higher CD8+ count in the epithelium have a higher DFS. Abbreviations: OS = overall survival, DFS = disease free survival.

higher levels of CD3+, CD4+, CD8+ and FOXP3+ lymphocytes and expression of PD-L1. These findings may reflect a higher level of inflammation and immune tolerance in these patients. Lin et al have shown a correlation with high PD-L1 expression and metastasis and poor prognosis in OTSCC [30]. However the effect of smoking on overall prognosis in oral cavity squamous cell carcinoma is controversial [31,32].

Interestingly, we found a significant interaction between the number of infiltrating CD8+ cells and adjuvant radiotherapy on both OS and DFS. High numbers of infiltrating CD8+ TILs portend a worse prognosis specifically for patients treated with adjuvant radiotherapy in this cohort. While previous studies have associated a high CD8+ count with a better prognosis, few studies have focused on the spatial distribution of CD8+ (and other immune cells) in OTSCC with large patient sample sizes [33–37]. Some studies have shown increased tumor recurrence in patients with higher infiltrating CD8+ cells [38,39], while others have shown that CD8+ count does not impact prognosis and that the ratio of CD8+ cells to regulatory immune cells is more prognostic instead [40,41]. There is evidence that radiation alters the ratios of various immune cells [29,42]. We speculate that while abundant TILs counteract tumor progression, radiotherapy may alter the tumor microenvironment so that the tumor could evade detection by the immune system and avoid elimination. This hypothesis generating result will require additional validation studies and mechanistic analysis.

Further studies of the immune microenvironment of OTSCCs will be needed to determine the prognostic and predictive value and clinical utility of potential biomarkers. These future studies may employ a version of the computer-assisted image analysis that we have evaluated in this study. In order to produce robust results, important findings from our study should be taken into consideration, such as the need for close proximity of pan-cytokeratin-stained sections to create a mask for the purpose of automated tissue compartment segmentation. To circumvent this issue, future studies may also employ immunofluorescence imaging and chromogenic multiplexed immunohistochemistry [43], which could produce improved localization of immune markers. In addition, obtaining samples from both the tumor core and the tumor invasive margin may provide further prognostic information [44,45].

Declaration of Competing Interest

Each author confirms there are no business relationships that might lead to a conflict of interest nor any other competing interests.

Acknowledgments

This study was supported by a Strategic Training in Transdisciplinary Radiation Science for the 21st Century (STARS21) training program fellowship awarded to SLL. SVB is supported by the Gattuso-Slaight Personalized Cancer Medicine Fund at the Princess Margaret Cancer Centre. We acknowledge the support from the Princess Margaret Cancer Foundation and the Princess Margaret Cancer Center Head & Neck Translational Program, with philanthropic funds from the Bartley-Smith/Wharton Family, The Joe & Cara Finley Center for Head & Neck Cancer Research, Dr. Mariano Elia, and Gordon Tozer.

Disclosure of interest

Authors have no disclosures.

Appendix A. Supplementary data

Supplementary data to this article can be found online at https://doi.org/10.1016/j.ctro.2019.05.001.

References

[1] Tirelli G, Gatto A, Boscolo Nata F, Bussani R, Piccinato A, Marcuzzo AV, et al. Prognosis of oral cancer: a comparison of the staging systems given in the 7th and 8th editions of the American Joint Committee on Cancer Staging Manual. Br J Oral Maxillofac Surg 2018;56:8–13. https://doi.org/10.1016/j.bjoms.2017.11.009.

[2] Majumdar B, Patil S, Sarode SC, Sarode GS, Rao RS. Clinico-pathological prognosticators in oral squamous cell carcinoma: An update 2057178X17738912. Transl Res Oral Oncol 2017;2. https://doi.org/10.1177/2057178X17738912.

[3] Markopoulos AK. Current aspects on oral squamous cell carcinoma. Open Dent J 2012;6:126–30. https://doi.org/10.2174/1874210601206010126.

[4] Li-Ting C, Chung-Ho C, Yi-Hsin Y, Pei-Shan H. The development and validation of oral cancer staging using administrative health data. BMC Cancer 2014;14:380. https://doi.org/10.1186/1471-2407-14-380.

[5] Galon J, Costes A, Sanchez-Cabo F, Kirilovsky A, Mlecnik B, Lagorce-Pagès C, et al. Type, density, and location of immune cells within human colorectal tumors predict clinical outcome. Science 2006;313:1960–4. https://doi.org/10.1126/science.1129139.

[6] Mandal R, Şenbabaoğlu Y, Desrichard A, Havel JJ, Dalin MG, Riaz N, et al. The head and neck cancer immune landscape and its immunotherapeutic implications. JCI Insight n.d.;1. doi:10.1172/jci.insight.89829.

[7] Balermpas P, Michel Y, Wagenblast J, Seitz O, Weiss C, Rödel F, et al. Tumour-infiltrating lymphocytes predict response to definitive chemoradiotherapy in head and neck cancer. Br J Cancer 2014;110:501–9. https://doi.org/10.1038/bjc.2013.640.

[8] Tumeh PC, Harview CL, Yearley JH, Shintaku IP, Taylor EJM, Robert L, et al. PD-1 blockade induces responses by inhibiting adaptive immune resistance. Nature 2014;515:568–71. https://doi.org/10.1038/nature13954.

[9] Taylor CR, Levenson RM. Quantification of immunohistochemistry—issues concerning methods, utility and semiquantitative assessment II. Histopathology 2006;49:411–24. https://doi.org/10.1111/j.1365-2559.2006.02513.x.

[10] Simon R, Sauter G. Tissue microarray (TMA) applications: implications for molecular medicine. Expert Rev Mol Med 2003;5:1–12. https://doi.org/10.1017/S1462399403006781.

[11] Psyrri A, Lee J-W, Pectasides E, Vassilakopoulou M, Kosmidis EK, Burtness BA, et al. Prognostic biomarkers in phase II trial of cetuximab-containing induction and chemoradiation in resectable HNSCC: eastern cooperative oncology group E2303. Clin Cancer Res 2014;20:3023–32. https://doi.org/10.1158/1078-0432.CCR-14-0113.

[12] Velcheti V, Schalper KA, Carvajal DE, Anagnostou VK, Syrigos KN, Sznol M, et al. Programmed death ligand-1 expression in non-small cell lung cancer. Lab Invest 2014;94:107–16. https://doi.org/10.1038/labinvest.2013.130.

[13] Halama N, Zoernig I, Spille A, Westphal K, Schirmacher P, Jaeger D, et al. Estimation of immune cell densities in immune cell conglomerates: an approach for high-throughput quantification. PLoS One 2009;4:. https://doi.org/10.1371/journal.pone.0007847e7847.

[14] Väyrynen JP, Vornanen JO, Sajanti S, Böhm JP, Tuomisto A, Mäkinen MJ. An improved image analysis method for cell counting lends credibility to the prognostic significance of T cells in colorectal cancer. Virchows Arch 2012;460:455–65. https://doi.org/10.1007/s00428-012-1232-0.

[15] Rizzardi AE, Johnson AT, Vogel RI, Pambuccian SE, Henriksen J, Skubitz AP, et al. Quantitative comparison of immunohistochemical staining measured by digital image analysis versus pathologist visual scoring. Diagn Pathol 2012;7:42. https://doi.org/10.1186/1746-1596-7-42.

[16] Angell HK, Gray N, Womack C, Pritchard DI, Wilkinson RW, Cumberbatch M. Digital pattern recognition-based image analysis quantifies immune infiltrates in distinct tissue regions of colorectal cancer and identifies a metastatic phenotype. Br J Cancer 2013;109:1618–24. https://doi.org/10.1038/bjc.2013.487.

[17] Adelstein D, Gillison ML, Pfister DG, Spencer S, Adkins D, Brizel DM, et al. Guidelines insights: head and neck cancers, Version 2.2017. J Natl Compr Canc Netw 2017;15:761–70. https://doi.org/10.6004/jnccn.2017.0101.

[18] McClelland RA, Finlay P, Walker KJ, Nicholson D, Robertson JFR, Blamey RW, et al. Automated quantitation of immunocytochemically localized estrogen receptors in human breast cancer. Cancer Res 1990;50:3545–50.

[19] Mattox AK, Lee J, Westra WH, Pierce RH, Ghossein R, Faquin WC, et al. PD-1 expression in head and neck squamous cell carcinomas derives primarily from functionally anergic CD4+ TILs in the presence of PD-L1+ TAMs. Cancer Res 2017;77:6365–74. https://doi.org/10.1158/0008-5472.CAN-16-3453.

[20] McLaughlin J, Han G, Schalper KA, Carvajal-Hausdorf D, Pelekanou V, Rehman J, et al. Quantitative assessment of the heterogeneity of PD-L1 expression in non–small-cell lung cancer. JAMA Oncol 2016;2:46–54. https://doi.org/10.1001/jamaoncol.2015.3638.

[21] Lejeune M, Jaén J, Pons L, López C, Salvadó M-T, Bosch R, et al. Quantification of diverse subcellular immunohistochemical markers with clinicobiological relevancies: validation of a new computer-assisted image analysis procedure. J Anat 2008;212:868–78. https://doi.org/10.1111/j.1469-7580.2008.00910.x.

[22] Alvarenga AW, Coutinho-Camillo CM, Rodrigues BR, Rocha RM, Torres LFB, Martins VR, et al. A comparison between manual and automated evaluations of tissue microarray patterns of protein expression. J Histochem Cytochem 2013;61:272–82. https://doi.org/10.1369/0022155413477661.

[23] Forrest R, Guthrie GJK, Orange C, Horgan PG, McMillan DC, Roxburgh CSD. Comparison of visual and automated assessment of tumour inflammatory infiltrates in patients with colorectal cancer. Eur J Cancer 2014;50:544–52. https://doi.org/10.1016/j.ejca.2013.11.003.

[24] Sayour EJ, McLendon P, McLendon R, Leon GD, Reynolds R, Kresak J, et al. Increased proportion of FoxP3+ regulatory T cells in tumor infiltrating lymphocytes is associated with tumor recurrence and reduced survival in patients with glioblastoma. Cancer Immunol Immunother 2015;64:419–27. https://doi.org/10.1007/s00262-014-1651-7.

[25] Pantanowitz L, Rimm D. Imaging and Quantitative Immunohistochemistry. Diagn. Immunohistochem. Theranostic Genomic Appl. 2nd ed., n.d., p. 877–84.

[26] Lange H. Digital pathology: a regulatory overview. Lab Med 2011;42:587–91. https://doi.org/10.1309/LMA2M9NQQF0ZCVHC.

[27] Galon J, Mlecnik B, Bindea G, Angell HK, Berger A, Lagorce C, et al. Towards the introduction of the 'Immunoscore' in the classification of malignant tumours. J Pathol 2014;232:199–209. https://doi.org/10.1002/path.4287.

[28] Pagès F, Mlecnik B, Marliot F, Bindea G, Ou F-S, Bifulco C, et al. International validation of the consensus Immunoscore for the classification of colon cancer: a prognostic and accuracy study. Lancet 2018;391:2128–39. https://doi.org/10.1016/S0140-6736(18)30789-X.

[29] Shimizu S, Hiratsuka H, Koike K, Tsuchihashi K, Sonoda T, Ogi K, et al. Tumor-infiltrating CD8+ T-cell density is an independent prognostic marker for oral squamous cell carcinoma. Cancer Med 2019;8:80–93. https://doi.org/10.1002/cam4.1889.

[30] Lin Y-M, Sung W-W, Hsieh M-J, Tsai S-C, Lai H-W, Yang S-M, et al. High PD-L1 expression correlates with metastasis and poor prognosis in oral squamous cell carcinoma. PLoS One 2015;10:. https://doi.org/10.1371/journal.pone.0142656e0142656.

[31] Durr ML, Li D, Wang SJ. Oral cavity squamous cell carcinoma in never smokers: analysis of clinicopathologic characteristics and survival. Am J Otolaryngol 2013;34:388–93. https://doi.org/10.1016/j.amjoto.2013.01.017.

[32] Durr ML, van Zante A, Li D, Kezirian EJ, Wang SJ. Oral tongue squamous cell carcinoma in never-smokers: analysis of clinicopathologic characteristics and survival. Otolaryngol Neck Surg 2013;149:89–96. https://doi.org/10.1177/0194599813482876.

[33] Kim HR, Ha S-J, Hong MH, Heo SJ, Koh YW, Choi EC, et al. PD-L1 expression on immune cells, but not on tumor cells, is a favorable prognostic factor for head and neck cancer patients. Sci Rep 2016;6:36956. https://doi.org/10.1038/srep36956.

[34] Wallis SP, Stafford ND, Greenman J. Clinical relevance of immune parameters in the tumor microenvironment of head and neck cancers. Head Neck 2015;37:449–59. https://doi.org/10.1002/hed.23736.

[35] Fridman WH, Pagès F, Sautès-Fridman C, Galon J. The immune contexture in human tumours: impact on clinical outcome. Nat Rev Cancer 2012;12:298–306. https://doi.org/10.1038/nrc3245.

[36] Balermpas P, Rödel F, Rödel C, Krause M, Linge A, Lohaus F, et al. CD8+ tumour-infiltrating lymphocytes in relation to HPV status and clinical outcome in patients with head and neck cancer after postoperative chemoradiotherapy: A multicentre study of the German cancer consortium radiation oncology group (DKTK-ROG). Int J Cancer 2016;138:171–81. https://doi.org/10.1002/ijc.29683.

[37] Zancope E, Costa NL, Junqueira-Kipnis AP, Valadares MC, Silva TA, Leles CR, et al. Differential infiltration of CD8+ and NK cells in lip and oral cavity squamous cell carcinoma. J Oral Pathol Med 2010;39:162–7. https://doi.org/10.1111/j.1600-0714.2009.00792.x.

[38] Wolf GT, Chepeha DB, Bellile E, Nguyen A, Thomas D, McHugh J. Tumor infiltrating lymphocytes (TIL) and prognosis in oral cavity squamous carcinoma: A preliminary study. Oral Oncol 2015;51:90–5. https://doi.org/10.1016/j.oraloncology.2014.09.006.

[39] Zhou C, Wu Y, Jiang L, Li Z, Diao P, Wang D, et al. Density and location of CD3+ and CD8+ tumor-infiltrating lymphocytes correlate with prognosis of oral squamous cell carcinoma. J Oral Pathol Med 2018;47:359–67. https://doi.org/10.1111/jop.12698.

[40] Tabachnyk M, Distel LVR, Büttner M, Grabenbauer GG, Nkenke E, Fietkau R, et al. Radiochemotherapy induces a favourable tumour infiltrating inflammatory cell profile in head and neck cancer. Oral Oncol 2012;48:594–601. https://doi.org/10.1016/j.oraloncology.2012.01.024.

[41] Cho Y-A, Yoon H-J, Lee J-I, Hong S-P, Hong S-D. Relationship between the expressions of PD-L1 and tumor-infiltrating lymphocytes in oral squamous cell carcinoma. Oral Oncol 2011;47:1148–53. https://doi.org/10.1016/j.oraloncology.2011.08.007.

[42] Tabachnyk M. Radiochemotherapy induces a favourable tumour infiltrating inflammatory cell profile in head and neck cancer n.d.;48:594–601.

[43] Huang W, Hennrick K, Drew S. A colorful future of quantitative pathology: validation of Vectra technology using chromogenic multiplexed immunohistochemistry and prostate tissue microarrays. Hum Pathol 2013;44:29–38. https://doi.org/10.1016/j.humpath.2012.05.009.

[44] Bryne M, Koppang HS, Lilleng R, Kjaerheim A. Malignancy grading of the deep invasive margins of oral squamous cell carcinomas has high prognostic value. J Pathol 1992;166:375–81. https://doi.org/10.1002/path.1711660409.

[45] Sandu K, Nisa L, Monnier P, Simon C, Andrejevic-Blant S, Bron L. Clinicobiological progression and prognosis of oral squamous cell carcinoma in relation to the tumor invasive front: impact on prognosis. Acta Otolaryngol (Stockh) 2014;134:416–24. https://doi.org/10.3109/00016489.2013.849818.